Biological Psychiatry

Review

The Potential of Myelin-Sensitive Imaging: Redefining Spatiotemporal Patterns of Myeloarchitecture

Casey Paquola and Seok-Jun Hong

ABSTRACT

Recent advances in magnetic resonance imaging (MRI) have paved the way for approximation of myelin content in vivo. In this review, our main goal was to determine how to best capitalize on myelin-sensitive imaging. First, we briefly overview the theoretical and empirical basis for the myelin sensitivity of different MRI markers and, in doing so, highlight how multimodal imaging approaches are important for enhancing specificity to myelin. Then, we discuss recent studies that have probed the nonuniform distribution of myelin across cortical layers and along white matter tracts. These approaches, collectively known as myelin profiling, have provided detailed depictions of myeloarchitecture in both the postmortem and living human brain. Notably, MRI-based profiling studies have recently focused on investigating whether it can capture interindividual variability in myelin characteristics as well as trajectories across the lifespan. Finally, another line of recent evidence emphasizes the contribution of region-specific myelination to large-scale organization, demonstrating the impact of myelination on global brain networks. In conclusion, we suggest that combining well-validated MRI markers with profiling techniques holds strong potential to elucidate individual differences in myeloarchitecture, which has important implications for understanding brain function and disease.

https://doi.org/10.1016/j.biopsych.2022.08.031

Myelin ensheathes axons of the central and peripheral nervous systems, providing the structural basis for fast and stable impulse propagation (1). The process of myelination is highly dynamic, involving rapid changes after even a few hours of a task and continuous reorganization across the lifespan (2–6). Indeed, the dynamic nature of myelin is thought to be central to its role in enabling flexible responses to rapidly changing environments and to maximizing the efficiency of neural communication (1). Elucidating the temporal dynamics and spatial patterns of myelination has been a topic of interest for over a century (7,8). As myelination throughout life is activity dependent (9), it has been theorized that the distribution of myelin reveals privileged microcircuits in the cortex that are relevant to understanding the structural basis of specific functions (10). Defining region-specific trajectories of myelination is thought to inform upon the maturational sequence of functional specialization in the brain (7,11), while region-specific breakdown of myelin in older age may reveal the structural underpinnings of cognitive decline (12). Classically, the spatial distribution of myelin has been described from postmortem study (13–16), but such approaches are inherently limited in characterizing intraindividual changes across time. Uncovering the spatiotemporal patterns of myelin necessitates in vivo imaging of myelin.

Magnetic resonance imaging (MRI) holds promise for enabling in vivo histology, whereby the cellular composition of living tissue may be discerned noninvasively. Crucially, MRI allows large, longitudinal cohort studies to track individual trajectories of tissue changes (17–19). Nevertheless, challenges remain for adoption of MRI for myelin mapping, as many previous approaches have been limited to indirectly measuring myelin via magnetic fields and confronted by the apparent discrepancy between imaging resolution and the size of myelin. New imaging sequences, contrasts, and biophysical models are helping to address these limitations, though not all MRI-derived myelin markers are equally valid. As interest in myelin mapping increases across foundational and clinical neuroscience, it is high time to discuss the validity of emerging techniques and identify promising avenues for future work.

In this review, we aim to demonstrate the significant contribution that myelin-sensitive imaging can make to understand the spatial patterns and dynamic changes of myeloarchitecture in the human brain. First, we lay the groundwork for how myelin markers are derived from MRI. Considering theoretical and histological validations, several multimodal approaches are highlighted that benefit disambiguation of myelin from other neurobiological factors. Next, we discuss the emergence of myelin profiling techniques, which provide nuanced characterization of the myeloarchitecture of cortical regions and white matter bundles. Finally, we highlight how several recent studies have capitalized on methodological improvements and in doing so have

ISSN: 0006-3223

advanced our understanding of how myeloarchitecture evolves across the lifespan.

DEVELOPING AND VALIDATING IN VIVO MYELIN MARKERS

Myelin, the lipid-rich material that insulates nerve fibers, is amenable to MRI measurement because it contributes to key determinants of MR relaxation times: water mobility and the interaction between water and macromolecules (20,21) (Figure 1A). Bound water produces shorter longitudinal (T1) and transverse (T2) relaxation times than free water (e.g., in cerebrospinal fluid) (Figure 1Aiii). As the primary location of bound water in the brain, myelin water has been shown to have distinctively short T1 and T2 relaxation times (30,31). However, looking across brain tissue types, the dominant source of T1 contrast are lipids (32). Cholesterol and cerebroside, in particular, both rich in myelin, are related to T1 shortening (20,33), which produces the distinctive appearance of gray and white matter in T1 images. In contrast, diffusion-weighted imaging targets anisotropy of hindered water (e.g., in axons or extracellular spaces), using multiple diffusion echo gradients to sensitize the MR signal to the random motion of water molecules. While myelin modulates anisotropy, for example by

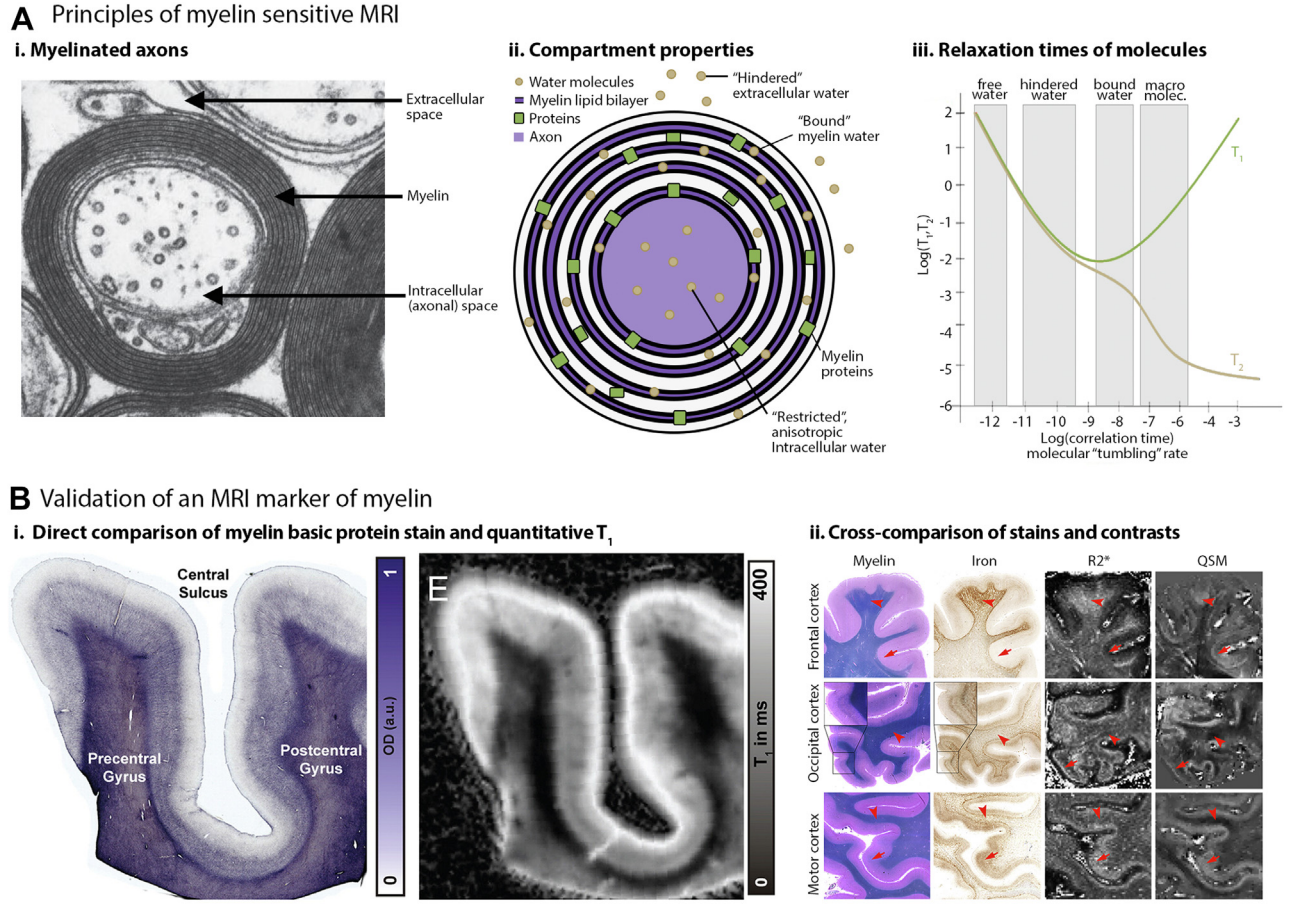

Figure 1. Sensitivity of magnetic resonance imaging (MRI) contrasts to myelin. **(A) (i)** Electron micrograph of a myelinated axon in the central nervous system (22). **(ii)** The schematic depicts distinctive features of myelinated axons that make them susceptible to MRI. [Adapted from Min *et al.* (23).] Myelin is composed of lipids (70%–85%) and proteins (15%–30%) (22). Water molecules are bound in the myelin sheath, which contrasts with the more motile water molecules in intra- and extracellular spaces [described as restricted and hindered water, respectively (24)]. **(iii)** T1 and T2 vary as a function of molecular tumbling rate (defined by correlation time) (25). Thereby, water in different compartments as well as macromolecules may be distinguished by T1 and T2. Positions of molecules along the x-axis are approximate (26). While T2 decay of macromolecules is too quick to be captured by human MRI scanners (26), the difference in T2 decay of water in different compartments can enable identification of myelin water [see, for example, (27)]. **(B) (i)** An exemplar validation study, Stüber *et al.* (28) showed the similar pattern of myelin basic protein staining and quantitative T1 in the same tissue. **(ii)** Cross-correlation of multiple stains and multiple contrasts can help disambiguate the contribution of different neurobiological features to an MRI marker. Here, Hametner *et al.* (29) show that iron is linearly related to R2*, but iron and myelin interact to determine quantitative susceptibility mapping (QSM). For instance, in the frontal cortex, high myelin and high iron produce moderate QSM (top arrow), but low myelin and low iron also produce moderate QSM (lower arrow). In other words, the myelin and iron appear to cancel each other out, related to the diamagnetism of myelin (lowers QSM) and paramagnetism of iron (increases QSM). Notably, the study showed that removing the contribution of iron from the QSM resulted in a strong correlation of QSM with myelin.

decreasing the permeability of axons, its effects on water diffusion are minimal (34). Therefore, classic diffusion-based measures are not posited as specific proxies for myelin. Turning to the macromolecular makeup of myelin, its protein and lipid composition render it diamagnetic. This distinctive property may be detected by combining the magnitude and phase maps from a gradient echo sequence, known as susceptibility mapping (35,36). This technique can identify susceptibility anisotropy created by ordered molecular structures such as myelin sheath, offering a new opportunity for clinical phenotyping of neurological disorders such as multiple sclerosis, Parkinson's disease, Alzheimer's disease, and Huntington's disease (35–38).

While the spatial resolution of myelin-sensitive MRI techniques has become increasingly higher with advanced hardware and sequence development [~500 μm, (39)], it is still at a relatively coarse level, such that each voxel likely includes multiple tissue types, contaminating the purity of its signal. Biophysical models can theoretically disentangle such heterogeneous signal sources and potentially enhance specificity to myelin. For example, myelin water fraction (MWF) is based on the fact that in the central nervous system, the T2 signal decay follows a multiexponential curve (30). By fitting the decay curve using least-square methods, these models can distinguish the myelin water pool, with ultrashort T2 decay, from the nonmyelin water pool (Figure 1Aiii). In contrast, magnetization transfer (MT) indirectly measures myelin based on the exchange and cross-relaxation between macromolecules (found predominantly in myelin) and water (40,41). Longitudinal relaxation rate (R1, also reported as 1/T1) is similarly driven by the cross-relaxation of lipids and water (33). Overall, this nonexhaustive summary of imaging contrasts and biophysical models serves to demonstrate that the influence of myelin on water mobility, as well as the lipid composition of myelin, allow sensitization of the MR signal to myelin in various ways with different assumptions, complexity, and presumed specificity.

Empirical validation has been essential to support the myelin sensitivity of the MR markers described above. The principal approach for validation is comparison with myelin-specific staining in the same tissue. Early studies described the correspondence of T1-weighted imaging contrasts with myelin distribution, such as distinctive myeloarchitectural features (e.g., stria of Gennari) or highly myelinated areas (e.g., primary sensory areas and middle temporal visual area) (42–46). The potential of myelin-sensitive imaging was further established by showing reduced values in individuals with multiple sclerosis (47–49), nonhuman animals without myelin basic protein (shiverer mouse) (50,51) or myelin proteolipid protein (shaking pup) (52), and rodents with cuprizole-induced demyelination (53,54). More recently, statistical approaches have been used to estimate the correlation between MRI markers and the degree of myelin staining, comparing many matched samples across regions and/or across individuals (Figure 1Bi). Collating such studies, several recent meta-analyses have found that many MRI markers are positively correlated with myelin content (55–57). MWF and MT approaches exhibit the highest sensitivity to myelin, but effect sizes are heterogeneous. The heterogeneity in estimates, which produces wide confidence intervals and overlapping prediction estimates across MRI markers, suggests that no single MRI marker may currently be considered the ideal myelin measure (55–57). Further studies are necessary to determine the interaction of MRI markers with influential methodological parameters, such as histological processing, sampling in gray or white matter, and statistical design. Alternative approaches include comparing MRI markers to oligodendrocyte- or myelin-related genes derived from brain transcriptomics. Such comparisons performed using T1-weighted/T2-weighted (T1w/T2w) scans suggest enrichment for myelin-related genes, but the association with myelin is not specific, nor is it the strongest enrichment present for T1w/T2w (58,59). This approach has also been extended to other MRI markers such as MT and MWF by comparing transcriptomic maps in one set of subjects [e.g., Allen Human Brain Atlas; (60)] to imaging maps in another set of subjects. Associations of these MRI markers with myelin-related genes and oligodendrocytes have been reported, though effect sizes tend to be small ($r < 0.4$) (61,62), as may be expected due to the confounding influence of interindividual differences, especially when the samples are not age matched.

The utility of myelin-sensitive imaging is also dependent on reliability. Test-retest reliability is high (intraclass correlation coefficient > 0.8) for many proposed myelin markers, including T2-derived MWF, quantitative MT, R1, and calibrated T1w/T2w ratio, but more moderate for other markers (intraclass correlation coefficient 0.5–0.8; e.g., MTR and raw T1w/T2w) (63–68). While supporting a certain level of consistency of these markers, the estimates are mostly derived from moderate sample sizes (average $n = 24$). More systematic efforts to optimize these metrics based on a larger population and different sites are therefore required to confirm the high reliability of their use in an actual clinical setting. Notably, recent work has demonstrated that T2-derived MWF, quantitative MT, and R1 have good intersite reliability (65,67,69). This evidence further bolsters their potential to become reproducible and clinically translatable biomarkers that are especially relevant to neurological disorders with a well-defined myelin pathology, such as multiple sclerosis, and psychiatric disorders with likely myelin alterations, such as schizophrenia (70).

Future work may benefit from multimodal imaging, whereby the combination of several MRI markers can enhance in vivo approximation of myelin distribution. Indeed, discrimination of normal myelin, demyelination, and remyelinated lesions in mice is improved by using the combination of 3 contrasts (T1w, T2w, and MTR; 95% accuracy) (71). The combination of susceptibility mapping with T2* (or R2*) can help to disambiguate myelin from iron (72) (Figure 1Bii). Myelin and iron often colocalize in the cortex and additively contribute to certain MR contrasts (e.g., increase in R2*) (73). However, they have opposing effects on resonance frequency (diamagnetic and paramagnetic, respectively), which may be detected by susceptibility mapping, and differ across tissue types, such as deep gray matter versus white matter (72). Consequently, contrasting R2* with susceptibility maps may provide a more specific MRI marker of myelin (29,74,75). Notably, other multimodal approaches, such as T1w/T2w (46) and T2*/B0 (76), use the commonalities of myelin and iron to characterize cortical microstructure with indiscriminate applicability to either source.

Multimodal protocols can also enable quantification of myelin sheath thickness relative to the thickness of myelinated

axon, namely the g-ratio (77). Known to be influential on conduction speed (78–80), the g-ratio is assessed using axonal volume and myelin volume fractions, which may be proxied in vivo using diffusion models, such as neurite orientation dispersion and density imaging (24), with myelin-sensitive imaging, such as MT. Notably, g-ratio values derived from MRI closely approximate g-ratio values calculated with electron microscopy, outperforming estimates of axonal volume and myelin volume fractions that come from each imaging modality separately (81). Therefore, while multimodal imaging approaches require extra consideration of theoretical assumptions and modality-specific distortions (82), this work demonstrates that combining modalities can benefit quantitative evaluation of myelin in vivo.

Overall, sensitivity, specificity, and reliability are important considerations in selecting a myelin-sensitive imaging sequence. However, these must be balanced against more practical requirements that vary across studies, such as acquisition time, available field strength, and the desired spatial resolution. R1 mapping has emerged as a simple and efficient method for myelin-sensitive imaging, with whole-brain coverage in only 8 minutes (magnetization-prepared 2 rapid acquisition gradient-echo: 1 mm on 3T, 0.7 mm on 7T) (67,83). Higher signal-to-noise ratio, spatial resolution, and image sharpness of R1 can be achieved using a recently developed multishot, inversion-recovery, echo planar imaging sequence, though the acquisition time is longer (20 minutes at 0.5 mm on 7T) (84). Toward multimodal imaging, the multiparameter mapping sequence provides 4 whole-brain quantitative maps (proton density, MTsat, R1, and R2*) in approximately 20 minutes (1 mm on 3T, 0.5 mm on 7T) (85,86). By reducing the resolution of the multiparameter mapping sequence to 1.6 mm on 3T, the acquisition time may be reduced to less than 10 minutes (87). Finally, recent developments with fast acquisition with spiral trajectory T2 imaging allow for whole-brain MWF, which exhibits high variability across white matter (88), to be captured in 10 minutes (1 mm on 3T) (89).

MYELIN PROFILING

A major advantage of myelin-sensitive MRI is the ability to explore myeloarchitecture in 3 dimensions. Myelin profiling, the measurement of myelin along biologically meaningful anatomical axes, is inspired by classic histology but benefits significantly from the 3-dimensional nature of MRI. While profiling in histological sections must follow the cutting plane, myelin profiling with MRI enables characterization of myelin along the natural courses of the cortex (from pial to white matter boundary) and along white matter tracts.

The origins of myelin profiling can be traced to the start of the 20th century. Around that time, several researchers developed myeloarchitectonic atlases of the cortex (8,15,16,90). In each case, cortical areas were delineated with respect to the vertical arrangement of myelinated fibers (Figure 2Ai). Myelinated fibers produce distinctive striations in the cortex, allowing categorization of types and the approximation of areal borders [see (97) for an excellent review]. Beyond qualitative types, histological studies have also used a photometric slice-capturing technique by which myeloarchitecture may be more quantitatively compared across the cortex based on myelin density across cortical depths (98). Hopf (91,92,99) showed that this quantitative approach allows comparison of distributed areas, elucidating large-scale patterns of myeloarchitectural change (Figure 2Aii). In particular, he demonstrated that myelin content decreases with distance from primary sensory and motor areas, with the lowest levels in the paralimbic cortex, such as the medial orbitofrontal cortex. Legacy data from these classic studies has the potential to serve as a histological gold standard to validate contemporary in vivo myelin-sensitive imaging. However, the accessibility of such datasets has been severely limited, in part due to their qualitative reporting and the 2-dimensional illustrations of the brain that are incompatible with modern neuroimaging. Recently, leveraging seminal meta-analyses of the Vogt-Vogt school (93), a myelin-based cortical parcellation was generated for neuroimaging analysis, whereby the parcel boundaries represent histology-derived estimates of myelin (Figure 2Aiii). Notably, the atlas also incorporates intracortical myelin profiles of multiple cortical areas based on Hopf's photometric studies, providing a unique resource to bridge ex vivo and in vivo imaging studies (94) (https://bic.mni.mcgill.ca/~noel/noel-myelin).

Depthwise profiling of cortical myelin, pioneered in histological studies, has been increasingly adopted by in vivo imaging (100–102). In a typical workflow, cortical surfaces are segmented using a standard T1w image, multiple intracortical surfaces are generated between the pial and white matter boundaries, and then the intensities of a coregistered myelin-sensitive image are sampled along the intracortical surfaces at matched vertices [code for protocol may be found in (103)] (Figure 2Bi). While depthwise profiling is agnostic to cortical layers, it is important to note that the vertical arrangement of cells and myelinated fibers varies with cortical curvature (104). As such, depthwise profiling approaches can use equivolumetric surface generation to account for these effects and minimize the influence of curvature on profiles (105). Another key concern is resolution. Dinse *et al.* (39) showed that distinctive features within intracortical profiles, such as turning points, disappear at lower resolutions (toward 1 mm) (Figure 2Bii), but areal differences remain evident. Areal differences are more pronounced at 0.4- to 0.5-mm resolution, which is increasingly feasible for whole-brain neuroimaging studies [e.g., 7T magnetization-prepared 2 rapid acquisition gradient-echo (83)]. Furthermore, Dinse *et al.* (39) showed that areas are best discriminated by combining mean intensity and profile shape differences rather than using either feature alone, reinforcing the benefit of using profiles to describe myeloarchitecture. These features (mean and shape) represent unique axes of cortical differentiation (Figure 2Biii) (95). Mean decreases with distance from primary sensory and motor areas and is lowest in frontal and temporal poles, in line with histological evidence (91,92). Shape is often summarized by profile skewness, a parameter adopted from cytoarchitectural histology (106), which pertains to the balance of intensities in upper versus lower layers. For MT-derived intracortical profiles, primary sensory-motor areas exhibit negative skewness, which is related to the gradual increase in MT across cortical depths, whereas cingulate and inferior temporal areas exhibit high skewness, which is related to relatively flat profiles with a sudden uptick in MT in the deepest layers (Figure 2Biii).

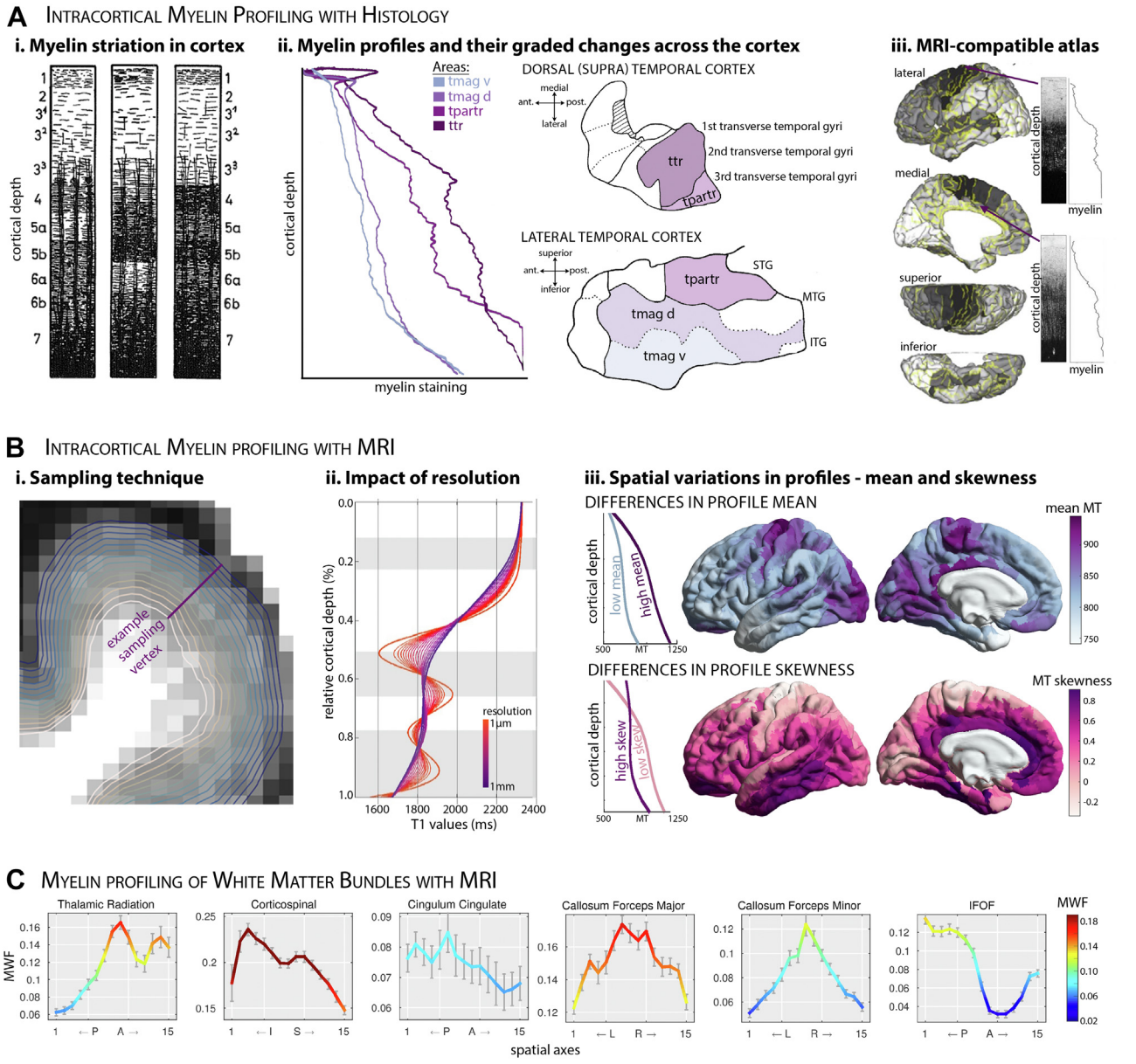

Figure 2. Myelin profiling. **(A) (i)** Classic drawings of myelin-stained cortical sections highlight how cortical areas differ with regard to myelin striation, signifying the potential to characterize areas with respect to depthwise variations in myelin density. [Reproduced with permission from Hopf *et al.* (91).] **(ii)** Histology-derived myelin profiles from different areas (left). Comparing profiles to areal positions (right) reveals a large-scale gradient in the myeloarchitecture; in this case "confirming steplike decrease in myelin content with increasing distance from the auditory region" (92). Based on the area-naming convention of the original text: tmag d, subregio temporalis magna dorsalis; tmag m, subregio temporalis magna ventralis; tpartr, regio temporalis paratransversa; ttr, regio temporalis transversa (primary auditory area). Additional anatomical landmarks are as follows: ITG, inferior temporal gyrus; MTG, middle temporal gyrus; STG, superior temporal gyrus. [Reproduced with permission from Hopf *et al.* (92); colors added to aid comparison between line and surface plots.] **(iii)** Histology-derived atlas of myeloarchitecture (93) generated on a magnetic resonance imaging (MRI)–compatible cortical surface (94), including intracortical myelin profiles for many areas, based on Hopf's photomicrograph studies. **(B) (i)** MRI-derived myelin profiling involves generating pial and white matter surfaces, generating equivolumetric surfaces between these 2 boundaries, and then sampling imaging intensities along a vertex that crosses the surfaces. **(ii)** Imaging resolution influences the smoothness of the profiles, yet distinctive elements of the profile shape remain evident even at 1-mm resolution. [Reproduced with permission from Dinse *et al.* (39).] **(iii)** The mean and skewness of MRI-derived myelin profiles capture unique information about myeloarchitecture as shown by the different patterns of each feature across the cortical surface. Cortical maps were generated using quantitative magnetization transfer (MT) imaging of healthy adolescents (95). Profiles on the left show extreme cases of high and low features, exemplifying how the features capture different aspects of the profiles. **(C)** Average myelin water fraction (MWF) across segments of white matter bundles. x-axes represent the dominant spatial dimension of the specific tract. Error bars show standard deviation across subjects, highlighting the robustness of tract profiles. IFOF, inferior fronto-occipital fasciculus. [Reproduced with permission from Baumeister *et al.* (96).]

Together, these variations in mean and skewness illustrate the existence of distinct, overlapping organizational axes of myeloarchitecture in the human cortex (Figure 2Biii). This work emphasizes the importance of incorporating multiple features of intracortical profiles in in vivo imaging studies to better understand myeloarchitectural differences and map large-scale patterns of cortical differentiation.

Extending the profiling approach past the gray/white matter boundary, recent work has evaluated the density of superficial white matter (SWM) (107). Historically, SWM (also known as the U-fiber system) has been difficult to study in vivo. The typical approach for fiber tracking, namely diffusion-weighted imaging, must be used at ultra-high-resolution for SWM (108) to account for its thinness and preponderance of crossing fibers (109). Alternatively, elevated iron levels in SWM (61) may be leveraged to target it with R2* (107). Immunohistochemical analysis of SWM has shown that its iron content colocalizes with oligodendrocytes, reinforcing the relevance of this approach to understanding myelin processes. Using an extended profiling approach, Kirilina *et al.* (107) identified higher density of SWM in frontotemporoparietal association areas than primary sensorimotor areas. This pattern notably differs from the regional distribution of intracortical myelin (Figure 2B), suggesting that together these profiling approaches can reveal the unique combinations of short- and long-range fibers in different cortical areas.

Myelin profiling can also shed light on ensheathment along white matter tracts. Electron microscopy studies of nonhuman animal brains have shown that myelin thickness can vary along axons (110,111). Relaxometry, diffusion-based, and g-ratio measures are known to vary along white matter tracts (81,112,113). Explicitly profiling MWF along white matter bundles, Baumeister *et al.* (96) recently identified characteristic patterns for each tract that could be replicated in all subjects (Figure 2C). This approach is more in its infancy than intracortical myelin profiling, and potential caveats, such as crossing fibers, need to be addressed (114). Even so, profiling approaches show promise for disambiguating subbundles within fasciculi (115). All in all, the profiling approach benefits from eschewing the assumption of uniform myelin distribution along white matter tracts and holds promise for offering greater sensitivity and specificity to inter- and intraindividual differences.

LINKING LOCAL MYELIN MARKERS TO CONNECTOME ORGANIZATION

Next, we ask how local myeloarchitecture, revealed by myelin profiling, contributes to the large-scale function of the human connectome. In particular, we highlight 2 avenues of recent work that have probed the interrelations between local myelin markers and structural connectome topology and network efficiency.

Contemporary perspectives emphasize that cortical gradients capture multifactorial changes in neurobiological features (58,116–119). The most prominent gradient, the sensory-fugal axis, runs from primary sensory areas toward limbic areas (103,116) and involves concomitant changes in myeloarchitecture, cytoarchitecture, connectivity, and function (118,120,121) (Figure 3Ai, ii). Many projections pass stepwise along the sensory-fugal axis, producing a set of parallel processing hierarchies, emanating from each primary sensory area (125) (Figure 3Aiii). Sequential processing through these hierarchies, with graded changes in underlying myelo- and cytoarchitecture, is thought to allow integration of information from several sources and gradual abstraction of neural code (116,118). We recently found that individual-level sensory-fugal axes may be defined by applying nonlinear dimensionality reduction to myelin profiles [(103); Figure 3B]. Thus, this approach links local properties of intracortical myeloarchitecture to global axes of cortical differentiation and provides a new foundation to map the dominant streams of information processing in individual human brains.

Turning toward white matter, the distribution of myelin influences the relationship between structural connectome topology and functional efficiency. The g-ratio, in particular, is a key contributor to conduction velocity (78). Thus, myelin-sensitive imaging can be combined with diffusion imaging to approximate conduction velocity across the connectome (126). In doing so, recent work has shown that the rich-club has lower g-ratio than local edges, which may enable faster and more efficient propagation within a set of densely connected but widely distributed regions (127). Initial work in Parkinson's disease also suggests that mapping myelin across the connectome can help to identify aberrant tracts that are associated with scores on motor performance tasks, signifying the potential importance of local myelin measures on more distributed brain function (128).

ADVANCING LIFESPAN RESEARCH WITH MYELIN-SENSITIVE IMAGING

The human lifespan is an ideal target for myelin research. Postmortem studies have long evidenced correlations between age and myelin, yet uncertainty remains regarding the principles of myeloarchitectural maturation. In vivo myelin-sensitive imaging offers the opportunity to track spatiotemporal patterns of myelin across the entire lifespan in large samples, helping to show how local changes can shape trajectories of larger-scale brain organization and their interrelations with other neurobiological features.

A principal challenge for lifespan research is determining the maturational sequence of myelination. As early as the 1870s, Flechsig (129) sought to prove that certain laws dictate the developmental sequence of pathways in the brain and spinal cord. Through detailed examination of white matter tracts and intracortical myelin in postmortem tissue, he showed that developmental myelination is protracted and asynchronous (7). The onset and duration of myelination (the myelogenetic cycle) varies across fiber systems and regions, with cycles spanning from in utero to adulthood. Kinney *et al.* (130) set forth the following general rules that explain the temporal patterns of myelination: 1) proximal pathways myelinate earlier and have shorter duration of myelination than distal pathways; 2) sensory pathways myelinate before motor pathways; 3) projection pathways myelinate earlier and have shorter myelination intervals than associative pathways; 4) myelination progresses from the central sulcus toward the poles; 5) occipital, followed by frontal, and then temporal poles myelinate; and 6) posterior frontoparietaloccipital areas have faster myelination than

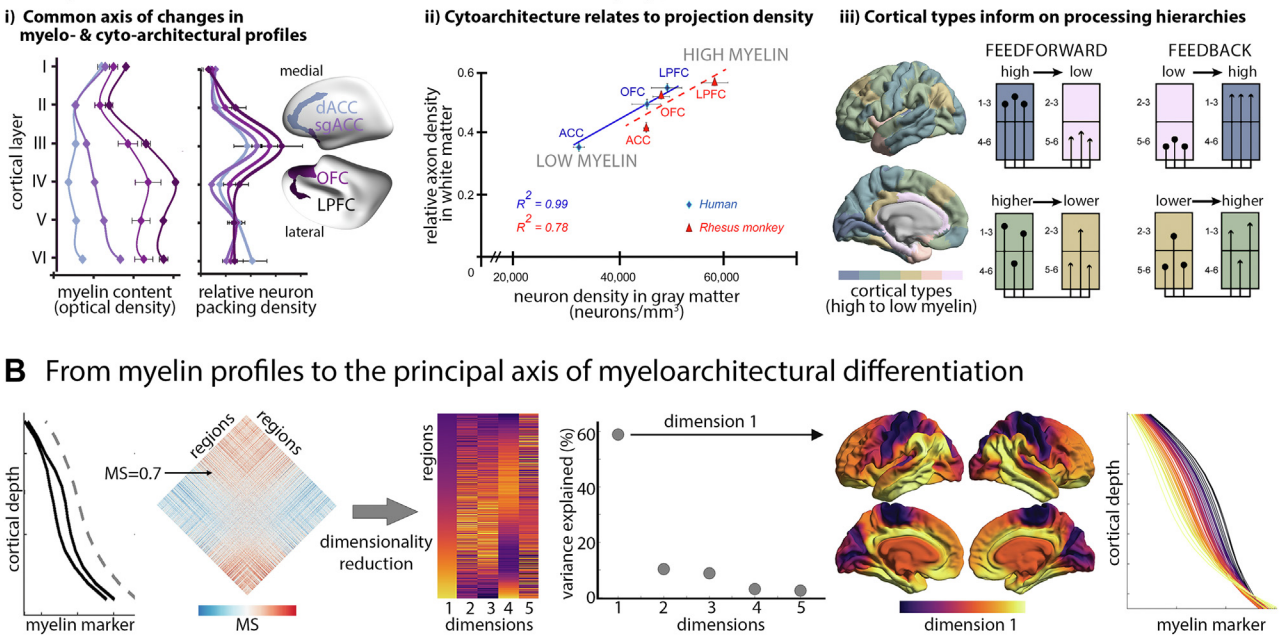

Figure 3. Relationship of local myelin to large-scale cortical organization. **(A) (i)** While myelin profiles (left) and cytoarchitectural profiles (right) differ in shape, they often capture a common spatial axis of changes across areas. For example, in the prefrontal cortex shown here, total myelin content and density of neurons in layer III increase along an axis that runs in a medial-lateral loop via the orbitofrontal cortex. dACC, dorsal anterior cingulate cortex; LPFC, lateral prefrontal cortex; OFC, orbitofrontal cortex; sgACC, subgenual anterior cingulate cortex. [Adapted with permission from Zikopoulos *et al.* (120). Line plot colors match the Brodmann areas delineated on the cortical surface (121).] **(ii)** Intracortical neuronal density is strongly correlated with the density of axons projecting from the cortical area, mirroring the spatial axis identified in Figure 3Ai and suggesting that intracortical myeloarchitecture is also associated with projection density [Reproduced with permission from Zikopoulos *et al.* (120). High and low myelin labels were added to aid interpretation.] **(iii)** Cortical types capture multifactorial changes in cyto- and myeloarchitecture that systematically vary along spatial axes (122). The relative type of 2 cortical areas indicates whether projections are in the feedforward (left) or feedback (right) direction as well as the laminar origin of projections. [Adapted with permission from Barbas and Rempel-Clower (123).] Thus, the relative myeloarchitecture of 2 cortical areas can index functional and structural characteristics of a neural network. **(B)** The principal axes of myeloarchitectural differentiation are resolved by first calculating myeloarchitectural similarity (MS) between regions based on the correlation of myelin profiles. Then, dimensionality reduction, typically diffusion map embedding (124), is applied to a matrix that contains MS between many cortical regions. The resultant dimensions reflect different spatial axes and are ranked according to the variance they explain in the MS matrix. In healthy adults, the first dimension runs from primary sensory and motor areas to limbic areas, closely approximating the sensory-fugal axis defined by postmortem histology (103). Coloring myelin profiles based on their position on dimension 1 illustrates how the axis reflects a decrease in myelin content as well as a shift from a concave to a convex curve. Notably, each dimension is sensitive to a different aspect of the myelin profile shape, related to myelin content at certain cortical depths. [Reproduced with permission from Paquola *et al.* (103).]

anterior frontotemporal regions. These large-scale rules provide a benchmark for imaging studies, which can in turn extend upon the postmortem research by providing nonbinary, quantitative assessment of myelin through investigation of healthy development and individual variability in large samples. For example, Kulikova *et al.* (131) demonstrated the potential of using multimodal parameters (R1, R2, and diffusion-based) to infer the maturational sequence of white matter bundles. Notably, the multivariate approach conformed to histological benchmarks with higher accuracy than did univariate approaches, supporting the utility of multimodal imaging for tracking myelin changes across the lifespan.

Recent studies have used MRI-derived myelin profiles, evaluated at multiple time points, to show how the patterns of myelin changes relate to brain organization at different life stages. Several theories have been proposed regarding the determinants of age-related myelin changes, such as the last-in/first-out hypothesis (132) and the spatial gradient hypothesis (130). Myelin-sensitive imaging is well positioned to test these hypotheses, given the possibilities to examine myelin across the entire brain and to track individual developmental trajectories. In infants, Grotheer *et al.* (133) showed that myelin levels at birth and spatial position contributed to age-related R1 changes in white matter bundles (Figure 4Ai). In certain tracts, speed of myelination is inversely correlated to the preexisting degree of myelin, whereas in other tracts, it is associated with spatial axes (Figure 4Aii). In adolescents, age-related changes in myelin also appear to reflect preexisting differences in intracortical myelin profiles (Figure 4Bi) (95). Specifically, areas that were less myeloarchitecturally distinct (relative to sensory and limbic areas) in early adolescence exhibit the strongest age-related changes throughout adolescence and young adulthood (Figure 4Bi). Notably, intracortical myelin profiles have linked local changes (i.e., myelination at a specific cortical depth) to large-scale patterns of myeloarchitectural maturation (Figure 4Bii). Beyond mere correlative effects, myelin profiles may hold predictive power for later life. Imaging studies suggest that

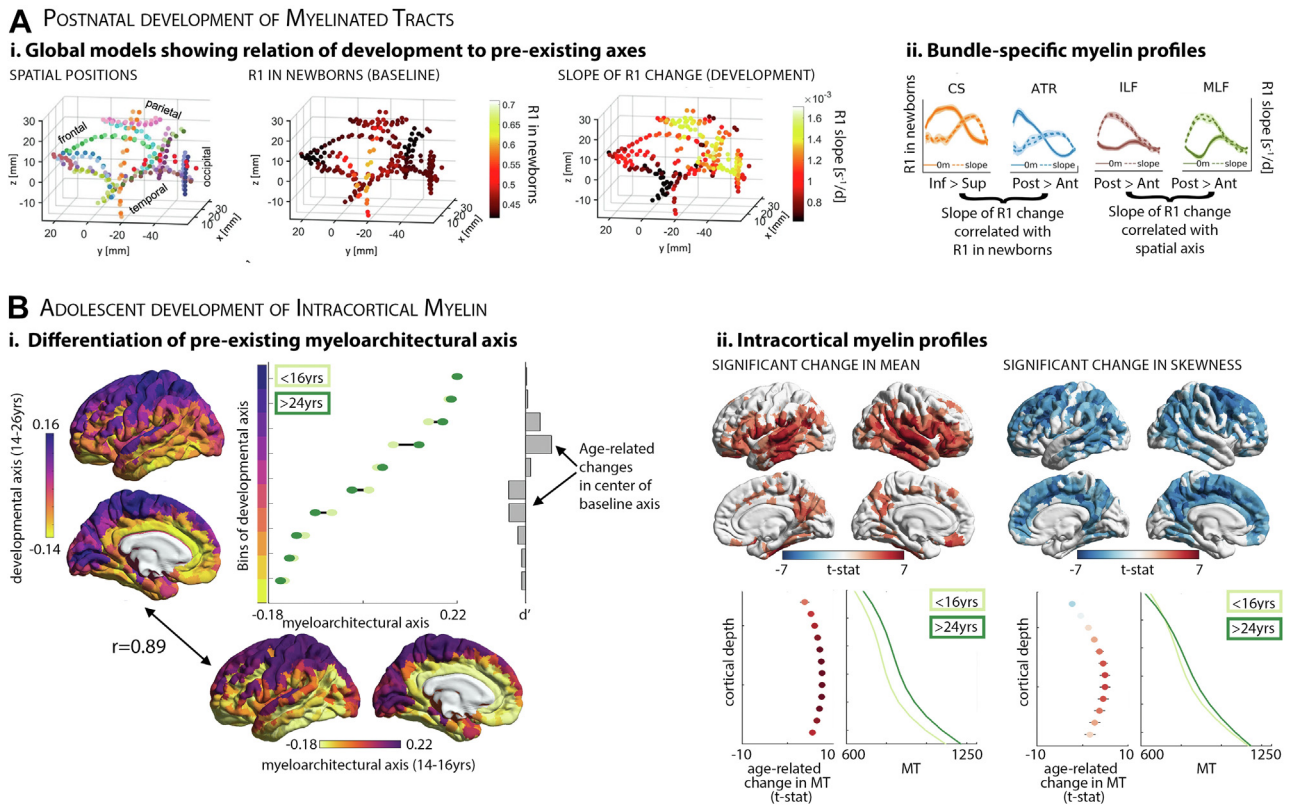

Figure 4. Myelin profiling approaches link local developmental changes to large-scale patterns of brain organization. **(A) (i)** Scatterplots represent sampling points along white matter bundles, colored by (left) bundle, (center) R1 in newborns and (right) development rate of R1 from 0 to 6 months. Across all points, development rate could be largely explained (67% of variance) by R1 in newborns and spatial position (anterior-posterior [ant-post] and inferior-superior [inf-sup] axes). [Reproduced with permission from Yeatman *et al.* (134).] **(ii)** Examining bundle-specific myelin, the developmental rate (slope, dotted line) is sometimes inversely correlated with R1 in newborns (0 m, full line) and at other times is correlated with a spatial axis (post-ant depicted as x-axis). [Reproduced with permission from Yeatman *et al.* (134).] ATR, anterior thalamic radiation; CS, cortico-spinal; ILF, inferior longitudinal fasciculus; MLF, middle longitudinal fasciculus. **(B) (i)** Regional variation in intracortical myelin profiles derived from magnetization transfer (MT) can be surmised by the myeloarchitectural axis. The more distant two regions are on the myeloarchitectural axis, the more dissimilar their intracortical myelin profiles are. In contrast, the more distant two regions are on the developmental axis, the more dissimilar their age-related changes in intracortical myelin profiles are. Notably, the baseline myeloarchitectural axis (derived from the earliest time points) and the developmental axis (calculated across the full age range) were strongly correlated (r = 0.89). Comparing myeloarchitectural axes at <16 and >24 years indicated that the most prominent age-related changes (Cohen's d effect size) were evident in the regions in the center of the developmental axis, suggesting differentiation of association cortex (orange) during this age range toward either the sensory (purple) or paralimbic (yellow) extremes. [Reproduced with permission from Paquola *et al.* (95).] **(ii)** Age-related changes in mean and skewness of myelin profiles shown on the cortical surfaces (threshold: q-value false discovery rate < 0.00625). Scatterplots show t statistic (mean ± SD) for age-related changes in MT intensity at each sampled cortical depth within significant regions. Mean increases were balanced across surfaces, whereas decreases in skewness were driven by preferential MT increases at mid-to-deeper surfaces. Line plots exemplify how myelin profiles change from the lowest to oldest age groups in significant regions. [Reproduced with permission from Paquola *et al.* (95).]

earlier patterns of myeloarchitecture can predict myelin decline in older age. Specifically, the speed of myelin accumulation in adolescence can index the speed of myelin decline in older age (i.e., fastest in, fastest out hypothesis) (134). Fine-grained spatial variations in later life have not yet been explored with profiling approaches, which could help to discern bundle- and region-specific differences. Together, these studies demonstrate how myelin-sensitive imaging is helping in testing hypotheses of how development and degeneration progress across the brain. This research suggests that a basic set of organizational axes may govern bundle- and region-specific myelination across the lifespan.

In parallel, multimodal approaches are helping to elucidate the interrelation of age-dependent changes in myelin with other neurobiological features. Particular attention has been paid to disentangling the contributions of myelin and axonal properties from diffusion-based parameters (135). Furthermore, the balance between myelin and axonal measures can inform clinically relevant aspects of development and degeneration. For instance, throughout infancy, the g-ratios of white matter bundles decrease logarithmically toward adult levels (136), likely related to the increasing thickness of myelin sheaths (137) and the efficient conduction speed in brain networks (138). At the other end of the lifespan, the equilibrium between remyelination, myelin degradation, and axonal loss can be approximated by multiparameter decomposition of T2 and may help indicate healthy versus pathological aging (12,139).

CONCLUDING REMARKS AND FUTURE PERSPECTIVES

The neuroimaging field provides strong evidence that myelin may be evaluated with in vivo MRI. Various MRI markers of myelin have been validated by comparing their values to well-established myelin markers acquired in the same tissue (i.e., histology, immunochemistry, or electron microscopy). Theoretically and empirically, T2-derived MWF, quantitative MT, and R1 provide good specificity to myelin. More caution is warranted in interpreting contrasts without such validation as specific myelin markers (e.g., T1w/T2w). Identifying the optimal multimodal combinations that can disambiguate myelin from artifactual and naturally occurring confounds, such as iron, is an important line of future research.

Moving forward, complementary "wide" and "deep" studies can help advance understanding of myeloarchitectural changes across the lifespan. On the one hand, large cohort studies that span a wide age range and demographic spectrum can leverage efficient whole-brain, quantitative, myelin-sensitive sequences to confirm (or deny) whether laws of myelination (133) generalize across the population and to extend these laws to intracortical myelin and aging populations. On the other hand, ultra-high-field MRI studies can investigate attributes of myeloarchitecture that were previously only accessible through postmortem microscopy, such as laminar detail in the cortex (39) as well as myelin distribution along U-fibers (107) and deep white matter tracts (110). Ideally, such studies would focus on deeply phenotyping a few individuals with repeated scans, helping to reveal the dynamic intraindividual changes in myelin across short and long time frames.

Overall, a key advantage of progress in investigating myeloarchitecture in vivo is the ability to directly assess the relationship of myelin with function (10), cognition (140), behavior (141), and diseases (12,142). Previous MRI studies have shown that increases in myelin markers on specific tracts are associated with more mature activity patterns in certain brain regions, supporting the notion of concomitant maturation of myelin and function in the brain (143,144). Conversely, MRI markers of myelin degradation have been linked to cognitive decline in healthy older individuals and individuals with Alzheimer's disease (145). Further work is necessary to characterize the likely bidirectional relationship between myelin and brain function. "Wide" studies of myeloarchitecture across large cohorts will help establish the associations between regional myelin and cognitive skills, but "deep" approaches offer greater promise in disentangling their causal relationships. In particular, behavioral training and neurofeedback protocols may be able to reveal the dynamic intraindividual changes in myelin and brain activity that support cognitive development or decline (146).

Myelin-sensitive imaging has the potential to complement and advance upon current approaches for understanding psychiatric and neurological diseases, especially those with neurodevelopmental or neurodegenerative origins. Schizophrenia, for example, is associated with reduced oligodendrocytes and myelin-related gene expression [for review, see (147)]. However, the nature of dysmyelination in schizophrenia, especially its progression, remains a contentious issue. Hypotheses variably focus on abnormal neurodevelopment (148) or accelerated neurodegeneration (149). The above-discussed advances in myelin imaging, analytics, and lifespan research paved the way to accurately track and characterize aberrant age-related changes in myelin in individuals with schizophrenia, thereby disentangling competing theories, improving understanding of the etiology of the disease, and benefiting models of clinical course. Similar outcomes are now possible for a wide range of psychiatric and neurological diseases thanks to recent advances in myelin-sensitive imaging.

ACKNOWLEDGMENTS AND DISCLOSURES

CP was funded by Helmholtz Association's Initiative and Networking Fund through the Helmholtz International BigBrain Analytics and Learning Laboratory under the Helmholtz International Lab grant agreement InterLabs-0015 and the Deutsche Forschungsgemeinschaft (German Research Foundation) (Grant No. 491111487).

The authors report no biomedical financial interests or potential conflicts of interest.

ARTICLE INFORMATION

From the Institute of Neuroscience and Medicine, Forschungszentrum Jülich, Jülich, Germany (CP); Center for Neuroscience Imaging Research, Institute for Basic Science, Sungkyunkwan University, Suwon, South Korea (S-JH); Center for the Developing Brain, Child Mind Institute, New York, New York (S-JH); and the Department of Biomedical Engineering, Sungkyunkwan University, Suwon, South Korea (S-JH).

Address correspondence to Casey Paquola, Ph.D., at c.paquola@fz-juelich.de.

Received May 18, 2022; revised Aug 12, 2022; accepted Aug 30, 2022.

REFERENCES

1. Nave KA, Werner HB (2014): Myelination of the nervous system: Mechanisms and functions. Annu Rev Cell Dev Biol 30:503–533.
2. Bottes S, Jessberger S (2021): Live imaging of remyelination in the adult mouse corpus callosum. Proc Natl Acad Sci U S A 118: e2025795118.
3. Gibson EM, Purger D, Mount CW, Goldstein AK, Lin GL, Wood LS, *et al.* (2014): Neuronal activity promotes oligodendrogenesis and adaptive myelination in the mammalian brain. Science 344: 1252304–1252304.
4. Hill RA, Li AM, Grutzendler J (2018): Lifelong cortical myelin plasticity and age-related degeneration in the live mammalian brain. Nat Neurosci 21:683–695.
5. Hughes EG, Orthmann-Murphy JL, Langseth AJ, Bergles DE (2018): Myelin remodeling through experience-dependent oligodendrogenesis in the adult somatosensory cortex [No. 5]. Nat Neurosci 21:696–706.
6. Xiao L, Ohayon D, McKenzie IA, Sinclair-Wilson A, Wright JL, Fudge AD, *et al.* (2016): Rapid production of new oligodendrocytes is required in the earliest stages of motor-skill learning [No. 9]. Nat Neurosci 19:1210–1217.
7. Flechsig Of Leipsic P (1901): Developmental (myelogenetic) localisation of the cerebral cortex in the human subject. Lancet 158:1027–1030.
8. Kaes T (1907): Die Grosshirnrinde Des Menschen in Ihren Massen Und in Ihrem Fasergehalt. Ein Gehirnanatomischer Atlas. Jena: Gustav Fischer.
9. Baraban M, Mensch S, Lyons DA (2016): Adaptive myelination from fish to man. Brain Res 1641:149–161.
10. Turner R (2019): Myelin and modeling: Bootstrapping cortical microcircuits. Front Neural Circuits 13:34.

11. Yakovlev P, Lecours A (1967): The myelogenetic cycles of regional maturation of the brain. In: Minkowski A, editor. Regional Development of the Brain in Early Life. Oxford: Blackwell Publishing, 3–70.
12. Bartzokis G (2004): Age-related myelin breakdown: A developmental model of cognitive decline and Alzheimer's disease. Neurobiol Aging 25:5–18; author reply 49.
13. Dejerine J, Dejerine–Klumpke A (1895): Anatomie des centres nerveux. Paris: Rueff.
14. Meynert T, Sachs B (1885): Psychiatry: A clinical treatise on diseases of the Fore-brain. New York: G.P. Putnam's Sons.
15. Smith GE (1907): A New Topographical Survey of the Human Cerebral Cortex, being an Account of the Distribution of the Anatomically Distinct Cortical Areas and their Relationship to the Cerebral sulci. J Anat Physiol 41:237–254.
16. Vogt O (1910): Die myeloarchitektonische Felderung des Menschlichen Stirnhirns. J Psychol Neurol 15:221–232.
17. Somerville LH, Bookheimer SY, Buckner RL, Burgess GC, Curtiss SW, Dapretto M, *et al.* (2018): The Lifespan Human connectome Project in Development: A large-scale study of brain connectivity development in 5–21 year olds. Neuroimage 183:456–468.
18. Sudlow C, Gallacher J, Allen N, Beral V, Burton P, Danesh J, *et al.* (2015): UK Biobank: An open access resource for identifying the causes of a Wide Range of complex diseases of middle and old age. PLoS Med 12:e1001779.
19. Volkow ND, Boyle M (2018): Neuroscience of addiction: Relevance to prevention and treatment. Am J Psychiatry 175:729–740.
20. Kucharczyk W, Macdonald PM, Stanisz GJ, Henkelman RM (1994): Relaxivity and magnetization transfer of white matter lipids at MR imaging: Importance of cerebrosides and pH. Radiology 192:521–529.
21. Weiskopf N, Edwards LJ, Helms G, Mohammadi S, Kirilina E (2021): Quantitative magnetic resonance imaging of brain anatomy and in vivo histology [No. 8]. Nat Rev Phys 3:570–588.
22. Morell P, Quarles RH (1999): Myelin formation, structure and biochemistry: Basic Neurochemistry, 6th ed. Lippincott-Raven.
23. Min Y, Kristiansen K, Boggs JM, Husted C, Zasadzinski JA, Israelachvili J (2009): Interaction forces and adhesion of supported myelin lipid bilayers modulated by myelin basic protein. Proc Natl Acad Sci U S A 106:3154–3159.
24. Zhang H, Schneider T, Wheeler-Kingshott CA, Alexander DC (2012): NODDI: Practical in vivo neurite orientation dispersion and density imaging of the human brain. Neuroimage 61:1000–1016.
25. Besghini D, Mauri M, Simonutti R (2019): Time Domain NMR in Polymer Science: From the Laboratory to the Industry [No. 9]. Appl Sci 9:1801.
26. McRobbie DW, Moore EA, Graves MJ, Prince MR, editors. (2017): Getting in tune: Resonance and relaxation: MRI From Picture to Proton, 3rd ed. Cambridge: Cambridge University Press, 124-143.
27. Borich MR, MacKay AL, Vavasour IM, Rauscher A, Boyd LA (2013): Evaluation of white matter myelin water fraction in chronic stroke. NeuroImage Clin 2:569–580.
28. Stüber C, Morawski M, Schäfer A, Labadie C, Wähnert M, Leuze C, *et al.* (2014): Myelin and iron concentration in the human brain: A quantitative study of MRI contrast. NeuroImage 93:95–106.
29. Hametner S, Endmayr V, Deistung A, Palmrich P, Prihoda M, Haimburger E, *et al.* (2018): The influence of brain iron and myelin on magnetic susceptibility and effective transverse relaxation – A biochemical and histological validation study. NeuroImage 179:117–133.
30. MacKay A, Laule C, Vavasour I, Bjarnason T, Kolind S, Mädler B (2006): Insights into brain microstructure from the T2 distribution. Magn Reson Imaging 24:515–525.
31. Labadie C, Lee JH, Rooney WD, Jarchow S, Aubert-Frécon M, Springer CS Jr, Möller HE (2014): Myelin water mapping by spatially regularized longitudinal relaxographic imaging at high magnetic fields. Magn Reson Med 71:375–387.
32. Leuze C, Aswendt M, Ferenczi E, Liu CW, Hsueh B, Goubran M, *et al.* (2017): The separate effects of lipids and proteins on brain MRI contrast revealed through tissue clearing. Neuroimage 156:412–422.
33. Koenig SH (1991): Cholesterol of myelin is the determinant of gray-white contrast in MRI of brain. Magn Reson Med 20:285–291.
34. Beaulieu C (2002): The basis of anisotropic water diffusion in the nervous system – A technical review. NMR Biomed 15:435–455.
35. Deistung A, Schweser F, Reichenbach JR (2017): Overview of quantitative susceptibility mapping. NMR Biomed 30.
36. Liu C, Li W, Tong KA, Yeom KW, Kuzminski S (2015): Susceptibility-weighted imaging and quantitative susceptibility mapping in the brain. J Magn Reson Imaging 42:23–41.
37. Johnson EB, Parker CS, Scahill RI, Gregory S, Papoutsi M, Zeun P, *et al.* (2021): Altered iron and myelin in premanifest Huntington's disease more than 20 years before clinical onset: Evidence from the cross-sectional HD Young Adult Study. EBiomedicine 65:103266.
38. Bulk M, Abdelmoula WM, Nabuurs RJA, van der Graaf LM, Mulders CWH, Mulder AA, *et al.* (2018): Postmortem MRI and histology demonstrate differential iron accumulation and cortical myelin organization in early- and late-onset Alzheimer's disease. Neurobiol Aging 62:231–242.
39. Dinse J, Härtwich N, Waehnert MD, Tardif CL, Schäfer A, Geyer S, *et al.* (2015): A cytoarchitecture-driven myelin model reveals area-specific signatures in human primary and secondary areas using ultra-high resolution in-vivo brain MRI. NeuroImage 114:71–87.
40. Sled JG (2018): Modelling and interpretation of magnetization transfer imaging in the brain. NeuroImage 182:128–135.
41. Sled JG, Pike GB (2001): Quantitative imaging of magnetization transfer exchange and relaxation properties in vivo using MRI. Magn Reson Med 46:923–931.
42. Clark VP, Courchesne E, Grafe M (1992): In vivo myeloarchitectonic analysis of human striate and extrastriate cortex using magnetic resonance imaging. Cereb Cortex 2:417–424.
43. Barbier EL, Marrett S, Danek A, Vortmeyer A, van Gelderen P, Duyn J, *et al.* (2002): Imaging cortical anatomy by high-resolution MR at 3.0T: Detection of the stripe of Gennari in visual area 17. Magn Reson Med 48:735–738.
44. Bock NA, Kocharyan A, Liu JV, Silva AC (2009): Visualizing the entire cortical myelination pattern in marmosets with magnetic resonance imaging. J Neurosci Methods 185:15–22.
45. Geyer S, Weiss M, Reimann K, Lohmann G, Turner R (2011): Microstructural parcellation of the human cerebral cortex – From Brodmann's post-mortem map to in vivo mapping with high-field magnetic resonance imaging. Front Hum Neurosci 5:19.
46. Glasser MF, Van Essen DC (2011): Mapping human cortical areas in vivo based on myelin content as revealed by T1- and T2-weighted MRI. J Neurosci 31:11597–11616.
47. Jeong IH, Choi JY, Kim SH, Hyun JW, Joung A, Lee J, Kim HJ (2016): Comparison of myelin water fraction values in periventricular white matter lesions between multiple sclerosis and neuromyelitis optica spectrum disorder. Mult Scler 22:1616–1620.
48. Schmierer K, Scaravilli F, Altmann DR, Barker GJ, Miller DH (2004): Magnetization transfer ratio and myelin in postmortem multiple sclerosis brain. Ann Neurol 56:407–415.
49. Schmierer K, Tozer DJ, Scaravilli F, Altmann DR, Barker GJ, Tofts PS, Miller DH (2007): Quantitative magnetization transfer imaging in postmortem multiple sclerosis brain. J Magn Reson Imaging 26:41–51.
50. Ou X, Sun SW, Liang HF, Song SK, Gochberg DF (2009): The MT pool size ratio and the DTI radial diffusivity may reflect the myelination in shiverer and control mice. NMR Biomed 22:480–487.
51. Ou X, Sun SW, Liang HF, Song SK, Gochberg DF (2009): Quantitative Magnetization Transfer Measured Pool-Size Ratio Reflects Optic Nerve Myelin Content in ex vivo Mice. Magn Reson Med 61:364–371.
52. Samsonov A, Alexander AL, Mossahebi P, Wu YC, Duncan ID, Field AS (2012): Quantitative MR imaging of two-pool magnetization transfer model parameters in myelin mutant shaking pup. Neuroimage 62:1390–1398.

53. Thiessen JD, Zhang Y, Zhang H, Wang L, Buist R, Del Bigio MR, *et al.* (2013): Quantitative MRI and ultrastructural examination of the cuprizone mouse model of demyelination. NMR Biomed 26:1562–1581.
54. Turati L, Moscatelli M, Mastropietro A, Dowell NG, Zucca I, Erbetta A, *et al.* (2015): In vivo quantitative magnetization transfer imaging correlates with histology during de- and remyelination in cuprizone-treated mice. NMR Biomed 28:327–337.
55. Lazari A, Lipp I (2021): Can MRI measure myelin? Systematic review, qualitative assessment, and meta-analysis of studies validating microstructural imaging with myelin histology. NeuroImage 230: 117744.
56. Mancini M, Karakuzu A, Cohen-Adad J, Cercignani M, Nichols TE, Stikov N (2020): An interactive meta-analysis of MRI biomarkers of myelin. eLife 9:e61523.
57. van der Weijden CWJ, García DV, Borra RJH, Thurner P, Meilof JF, van Laar PJ, *et al.* (2021): Myelin quantification with MRI: A systematic review of accuracy and reproducibility. NeuroImage 226:117561.
58. Fulcher BD, Murray JD, Zerbi V, Wang XJ (2019): Multimodal gradients across mouse cortex. Proc Natl Acad Sci U S A 116:4689–4695.
59. Ritchie J, Pantazatos SP, French L (2018): Transcriptomic characterization of MRI contrast with focus on the T1-w/T2-w ratio in the cerebral cortex. NeuroImage 174:504–517.
60. Hawrylycz MJ, Lein ES, Guillozet-Bongaarts AL, Shen EH, Ng L, Miller JA, *et al.* (2012): An anatomically comprehensive atlas of the adult human brain transcriptome. Nature 489:391–399.
61. Whitaker KJ, Vértes PE, Romero-Garcia R, Váša F, Moutoussis M, Prabhu G, *et al.* (2016): Adolescence is associated with genomically patterned consolidation of the hubs of the human brain connectome. Proc Natl Acad Sci U S A 113:9105–9110.
62. Patel Y, Shin J, Drakesmith M, Evans J, Pausova Z, Paus T (2020): Virtual histology of multi-modal magnetic resonance imaging of cerebral cortex in young men. NeuroImage 218:116968.
63. Arshad M, Stanley JA, Raz N (2017): Test–retest reliability and concurrent validity of in vivo myelin content indices: Myelin water fraction and calibrated T1w/T2w image ratio. Hum Brain Mapp 38:1780–1790.
64. Nerland S, Jørgensen KN, Nordhøy W, Maximov II, Bugge RAB, Westlye LT, *et al.* (2021): Multisite reproducibility and test–retest reliability of the T1w/T2w-ratio: A comparison of processing methods. NeuroImage 245:118709.
65. Zhang L, Chen T, Tian H, Xue H, Ren H, Li L, *et al.* (2019): Reproducibility of inhomogeneous magnetization transfer (ihMT): A test–retest, multi-site study. Magn Reson Imaging 57:243–249.
66. Shams Z, Norris DG, Marques JP (2019): A comparison of in vivo MRI based cortical myelin mapping using T1w/T2w and R1 mapping at 3T. PLoS One 14:e0218089.
67. Haast RAM, Ivanov D, Formisano E, Uludağ K (2016): Reproducibility and reliability of quantitative and weighted T1 and T2* mapping for myelin-based cortical parcellation at 7 tesla. Front Neuroanat 10: 112–112.
68. Lévy S, Guertin MC, Khatibi A, Mezer A, Martinu K, Chen JI, *et al.* (2018): Test–retest reliability of myelin imaging in the human spinal cord: Measurement errors versus region- and aging-induced variations. PLoS One 13:e0189944.
69. Meyers SM, Vavasour IM, Mädler B, Harris T, Fu E, Li DKB, *et al.* (2013): Multicenter measurements of myelin water fraction and geometric mean T2: Intra- and intersite reproducibility. J Magn Reson Imaging 38:1445–1453.
70. Dietz AG, Goldman SA, Nedergaard M (2020): Glial cells in schizophrenia: A unified hypothesis. Lancet Psychiatry 7:272–281.
71. Merkler D, Boretius S, Stadelmann C, Ernsting T, Michaelis T, Frahm J, Brück W (2005): Multicontrast MRI of remyelination in the central nervous system. NMR Biomed 18:395–403.
72. Deistung A, Schäfer A, Schweser F, Biedermann U, Turner R, Reichenbach JR (2013): Toward in vivo histology: A comparison of quantitative susceptibility mapping (QSM) with magnitude-, phase-, and R2*-imaging at ultra-high magnetic field strength. NeuroImage 65:299–314.
73. Fukunaga M, Li TQ, van Gelderen P, de Zwart JA, Shmueli K, Yao B, *et al.* (2010): Layer-specific variation of iron content in cerebral cortex as a source of MRI contrast. Proc Natl Acad Sci U S A 107:3834–3839.
74. Lambrecht V, Hanspach J, Hoffmann A, Seyler L, Mennecke A, Straub S, *et al.* (2020): Quantitative susceptibility mapping depicts severe myelin deficit and iron deposition in a transgenic model of multiple system atrophy. Exp Neurol 329:113314.
75. Marques JP, Khabipova D, Gruetter R (2017): Studying cyto and myeloarchitecture of the human cortex at ultra-high field with quantitative imaging: R1, R2* and magnetic susceptibility. NeuroImage 147:152–163.
76. Cohen-Adad J, Polimeni JR, Helmer KG, Benner T, McNab JA, Wald LL, *et al.* (2012): T2* mapping and B0 orientation-dependence at 7T reveal cyto- and myeloarchitecture organization of the human cortex. NeuroImage 60:1006–1014.
77. Campbell JSW, Leppert IR, Narayanan S, Boudreau M, Duval T, Cohen-Adad J, *et al.* (2018): Promise and pitfalls of g-ratio estimation with MRI. NeuroImage 182:80–96.
78. Drakesmith M, Harms R, Rudrapatna SU, Parker GD, Evans CJ, Jones DK (2019): Estimating axon conduction velocity in vivo from microstructural MRI. NeuroImage 203:116186.
79. Rushton WA (1951): A theory of the effects of fibre size in medullated nerve. J Physiol 115:101–122.
80. Waxman SG, Bennett MVL (1972): Relative Conduction Velocities of Small Myelinated and Non-myelinated Fibres in the central nervous system [No. 85]. Nat New Biol 238:217–219.
81. Stikov N, Campbell JSW, Stroh T, Lavelée M, Frey S, Novek J, *et al.* (2015): In vivo histology of the myelin g-ratio with magnetic resonance imaging. Neuroimage 118:397–405.
82. Mohammadi S, Carey D, Dick F, Diedrichsen J, Sereno MI, Reisert M, *et al.* (2015): Whole-brain in-vivo measurements of the axonal G-ratio in a group of 37 healthy volunteers. Front Neurosci 9:441.
83. Marques JP, Kober T, Krueger G, van der Zwaag W, Van de Moortele P-FF, Gruetter R (2010): MP2RAGE, a self bias-field corrected sequence for improved segmentation and T1-mapping at high field. NeuroImage 49:1271–1281.
84. Sanchez Panchuelo RM, Mougin O, Turner R, Francis ST (2021): Quantitative T1 mapping using multi-slice multi-shot inversion recovery EPI. Neuroimage 234:117976.
85. Weiskopf N, Suckling J, Williams G, Correia MM, Inkster B, Tait R, *et al.* (2013): Quantitative multi-parameter mapping of R1, PD(*), MT, and R2(*) at 3T: A multi-center validation. Front Neurosci 7: 95–95.
86. McColgan P, Helbling S, Vaculčiaková L, Pine K, Wagstyl K, Attar FM, *et al.* (2021): Relating quantitative 7T MRI across cortical depths to cytoarchitectonics, gene expression and connectomics. Hum Brain Mapp 42:4996–5009.
87. Cooper G, Hirsch S, Scheel M, Brandt AU, Paul F, Finke C, *et al.* (2020): Quantitative multi-parameter mapping optimized for the clinical routine. Front Neurosci 14:611194.
88. Liu H, Rubino C, Dvorak AV, Jarrett M, Ljungberg E, Vavasour IM, *et al.* (2019): Myelin water atlas: A template for myelin distribution in the brain. J Neuroimaging 29:699–706.
89. Nguyen TD, Deh K, Monohan E, Pandya S, Spincemaille P, Raj A, *et al.* (2016): Feasibility and reproducibility of whole brain myelin water mapping in 4 minutes using fast acquisition with spiral trajectory and adiabatic T2prep (FAST-T2) at 3T. Magn Reson Med 76:456–465.
90. Campbell AW (1905): Histological Studies on the Localisation of Cerebral Function. Cambridge: University Press.
91. Hopf A (1968): Photometric studies on the myeloarchitecture of the human temporal lobe. J Hirnforsch 10:285–297.
92. Hopf A (1969): Photometric studies on the myeloarchitecture of the human parietal lobe. I. Parietal region. J Hirnforsch 11:253–265.
93. Nieuwenhuys R, Broere CAJ (2017): A map of the human neocortex showing the estimated overall myelin content of the individual architectonic areas based on the studies of Adolf Hopf. Brain Struct Funct 222:465–480.

94. Foit NA, Yung S, Lee HM, Bernasconi A, Bernasconi N, Hong S-J (2022): A whole-brain 3D myeloarchitectonic atlas: Mapping the Vogt–Vogt legacy to the cortical surface. Neuroimage 263: 119617.
95. Paquola C, Bethlehem RA, Seidlitz J, Wagstyl K, Romero-Garcia R, Whitaker KJ, *et al.* (2019): Shifts in myeloarchitecture characterise adolescent development of cortical gradients. eLife 8.
96. Baumeister TR, Kolind SH, MacKay AL, McKeown MJ (2020): Inherent spatial structure in myelin water fraction maps. Magn Reson Imaging 67:33–42.
97. Nieuwenhuys R, Broere CAJ, Cerliani L (2015): A new myeloarchitectonic map of the human neocortex based on data from the Vogt–Vogt school. Brain Struct Funct 220:2551–2573.
98. Braitenberg V (1962): A note on myeloarchitectonics. J Comp Neurol 118:141–156.
99. Hopf A (1968): Registration of the myeloarchitecture of the human frontal lobe with an extinction method. J Hirnforsch 10:259–269.
100. Trampel R, Ott DVM, Turner R (2011): Do the congenitally blind have a stria of Gennari? First intracortical insights in vivo. Cereb Cortex 21:2075–2081.
101. Tardif CL, Schäfer A, Waehnert M, Dinse J, Turner R, Bazin PL (2015): Multi-contrast multi-scale surface registration for improved alignment of cortical areas. NeuroImage 111:107–122.
102. Sprooten E, O'Halloran R, Dinse J, Lee WH, Moser DA, Doucet GE, *et al.* (2019): Depth-dependent intracortical myelin organization in the living human brain determined by in vivo ultra-high field magnetic resonance imaging. Neuroimage 185:27–34.
103. Paquola C, Vos De Wael R, Wagstyl K, Bethlehem RAI, Hong SJ, Seidlitz J, *et al.* (2019): Microstructural and functional gradients are increasingly dissociated in transmodal cortices. PLoS Biol Kennedy H editor 17:e3000284.
104. Bok ST (1929): Der Einfluß der in den Furchen und Windungen auftretenden Krümmungen der Großhirnrinde auf die Rindenarchitektur. Z gesamte Neurol Psychiatr 121:682–750.
105. Waehnert MD, Dinse J, Weiss M, Streicher MN, Waehnert P, Geyer S, *et al.* (2014): Anatomically motivated modeling of cortical laminae. NeuroImage 93:210–220.
106. Schleicher A, Amunts K, Geyer S, Morosan P, Zilles K (1999): Observer-independent method for microstructural parcellation of cerebral cortex: A quantitative approach to cytoarchitectonics. NeuroImage 9:165–177.
107. Kirilina E, Helbling S, Morawski M, Pine K, Reimann K, Jankuhn S, *et al.* (2020): Superficial white matter imaging: Contrast mechanisms and whole-brain in vivo mapping. Sci Adv 6.
108. Movahedian Attar F, Kirilina E, Haenelt D, Pine KJ, Trampel R, Edwards LJ, Weiskopf N (2020): Mapping short association fibers in the early cortical visual processing stream using in vivo diffusion tractography. Cereb Cortex 30:4496–4514.
109. Reveley C, Seth AK, Pierpaoli C, Silva AC, Yu D, Saunders RC, *et al.* (2015): Superficial white matter fiber systems impede detection of long-range cortical connections in diffusion MR tractography. Proc Natl Acad Sci U S A 112:E2820–E2828.
110. Giorgi PP, DuBois H (1980): Regional differences in thickness and metabolism of the myelin sheath along the optic nerve and tract of rabbit. Neuroscience 5:2013–2022.
111. Tomassy GS, Berger DR, Chen HH, Kasthuri N, Hayworth KJ, Vercelli A, *et al.* (2014): Distinct profiles of myelin distribution along single axons of pyramidal neurons in the neocortex. Science 344:319–324.
112. Jones DK, Deoni SC (2006): Visualization of absolute T1 and T2 along specific white matter tracts. Proc Int Soc Magn Reson Med 14:14.
113. Yeatman JD, Dougherty RF, Myall NJ, Wandell BA, Feldman HM (2012): Tract profiles of white matter properties: Automating fiber-tract quantification. PLoS One 7:e49790.
114. Schiavi S, Lu PJ, Weigel M, Lutti A, Jones DK, Kappos L, *et al.* (2022): Bundle myelin fraction (BMF) mapping of different white matter connections using microstructure informed tractography. NeuroImage 249:118922.
115. Schurr R, Zelman A, Mezer AA (2020): Subdividing the superior longitudinal fasciculus using local quantitative MRI. NeuroImage 208: 116439.
116. Mesulam MM (1998): From sensation to cognition. Brain 121:1013–1052.
117. Huntenburg JM, Bazin PL, Margulies DS (2018): Large-scale gradients in human cortical organization. Trends Cogn Sci 22:21–31.
118. Hilgetag CC, Goulas A, Changeux J-P (2022): A natural cortical axis connecting the outside and inside of the human brain. Netw Neurosci 1–10.
119. Paquola C, Amunts K, Evans A, Smallwood J, Bernhardt B (2022): Closing the mechanistic gap: The value of microarchitecture in understanding cognitive networks. Trends Cogn Sci 0.
120. Zikopoulos B, García-Cabezas MÁ., Barbas H (2018): Parallel trends in cortical gray and white matter architecture and connections in primates allow fine study of pathways in humans and reveal network disruptions in autism. PLoS Biol 16:e2004559.
121. García-Cabezas MÁ., Hacker JL, Zikopoulos B (2020): A protocol for cortical type analysis of the human neocortex applied on histological samples, the atlas of Von economo and Koskinas, and magnetic resonance imaging. Front Neuroanat 14:576015.
122. Pijnenburg R, Scholtens LH, Ardesch DJ, de Lange SC, Wei Y, van den Heuvel MP (2021): Myelo- and cytoarchitectonic microstructural and functional human cortical atlases reconstructed in common MRI space. NeuroImage 239:118274.
123. Barbas H, Rempel-Clower N (1997): Cortical structure predicts the pattern of corticocortical connections. Cereb Cortex 7:635–646.
124. Coifman RR, Lafon S (2006): Diffusion maps. Appl Comp Harmon Anal 21:5–30.
125. Felleman DJ, Van Essen DC (1991): Distributed hierarchical processing in the primate cerebral cortex. Cereb Cortex 1:1–47.
126. Mancini M, Tian Q, Fan Q, Cercignani M, Huang SY (2021): Dissecting whole-brain conduction delays through MRI microstructural measures. Brain Struct Funct 226:2651–2663.
127. Mancini M, Giulietti G, Dowell N, Spanò B, Harrison N, Bozzali M, Cercignani M (2018): Introducing axonal myelination in connectomics: A preliminary analysis of g-ratio distribution in healthy subjects. NeuroImage 182:351–359.
128. Boshkovski T, Cohen-Adad J, Misic B, Arnulf I, Corvol JC, Vidailhet M, *et al.* (2022): The myelin-weighted connectome in Parkinson's disease. Mov Disord 37:724–733.
129. Flechsig P (1876): Die Leitungsbahnen im Gehirn und Rückenmark des Menschen auf Grund entwicklungsgeschichtlicher Untersuchungen dargestellt. Engelmann.
130. Kinney HC, brody BA, Kloman AS, Gilles FH (1988): Sequence of central nervous system myelination in human infancy. II. Patterns of myelination in autopsied infants. J Neuropathol Exp Neurol 47:217–234.
131. Kulikova S, Hertz-Pannier L, Dehaene-Lambertz G, Buzmakov A, Poupon C, Dubois J (2015): Multi-parametric evaluation of the white matter maturation. Brain Struct Funct 220:3657–3672.
132. Raz N (2000): Aging of the brain and its impact on cognitive performance: Integration of structural and functional findings: The Handbook of Aging and Cognition, 2nd ed. Mahwah, NJ: Lawrence Erlbaum Associates Publishers, 1-90.
133. Grotheer M, Rosenke M, Wu H, Kular H, Querdasi FR, Natu VS, *et al.* (2022): White matter myelination during early infancy is linked to spatial gradients and myelin content at birth [No. 1]. Nat Commun 13:997.
134. Yeatman JD, Wandell BA, Mezer AA (2014): Lifespan maturation and degeneration of human brain white matter [No. 1]. Nat Commun 5:4932.
135. Nossin-Manor R, Card D, Morris D, Noormohamed S, Shroff MM, Whyte HE, *et al.* (2013): Quantitative MRI in the very preterm brain: Assessing tissue organization and myelination using magnetization transfer, diffusion tensor and T1 imaging. NeuroImage 64:505–516.
136. Dean DC, O'Muircheartaigh J, Dirks H, Travers BG, Adluru N, Alexander AL, Deoni SCL (2016): Mapping an index of the myelin

g-ratio in infants using magnetic resonance imaging. NeuroImage 132:225–237.

137. Schröder JM, Bohl J, von Bardeleben U (1988): Changes of the ratio between myelin thickness and axon diameter in human developing sural, femoral, ulnar, facial, and trochlear nerves. Acta Neuropathol 76:471–483.
138. Chomiak T, Hu B (2009): What is the optimal value of the g-ratio for myelinated fibers in the rat CNS? A theoretical approach. PLoS One 4:e7754.
139. Lynn JD, Anand C, Arshad M, Homayouni R, Rosenberg DR, Ofen N, *et al.* (2021): Microstructure of human corpus callosum across the lifespan: Regional variations in axon caliber, density, and myelin content. Cereb Cortex 31:1032–1045.
140. Raz N, Daugherty AM (2018): Pathways to brain aging and their modifiers: Free-radical-induced energetic and neural decline in senescence (FRIENDS) Model – A Mini-Review. Gerontology 64:49–57: Model - A.
141. Kaller MS, Lazari A, Blanco-Duque C, Sampaio-Baptista C, Johansen-Berg H (2017): Myelin plasticity and behaviour-connecting the dots. Curr Opin Neurobiol 47:86–92.
142. Stassart RM, Möbius W, Nave KA, Edgar JM (2018): The axon-myelin unit in development and degenerative disease. Front Neurosci 12:467.
143. Fornari E, Knyazeva MG, Meuli R, Maeder P (2007): Myelination shapes functional activity in the developing brain. NeuroImage 38:511–518.
144. Meissner TW, Genç E, Mädler B, Weigelt S (2021): Myelin development in visual scene-network tracts beyond late childhood: A multi-method neuroimaging study. Cortex 137:18–34.
145. Brickman AM, Meier IB, Korgaonkar MS, Provenzano FA, Grieve SM, Siedlecki KL, *et al.* (2012): Testing the white matter retrogenesis hypothesis of cognitive aging. Neurobiol Aging 33:1699–1715.
146. Sampaio-Baptista C, Neyedli HF, Sanders ZB, Diosi K, Havard D, Huang Y, *et al.* (2021): fMRI neurofeedback in the motor system elicits bidirectional changes in activity and in white matter structure in the adult human brain. Cell Rep 37:109890.
147. Takahashi N, Sakurai T, Davis KL, Buxbaum JD (2011): Linking oligodendrocyte and myelin dysfunction to neurocircuitry abnormalities in schizophrenia. Prog Neurobiol 93:13–24.
148. Weinberger DR (1996): On the plausibility of "the neurodevelopmental hypothesis" of schizophrenia. Neuropsychopharmacology 14(suppl):1S–11S.
149. Stone WS, Phillips MR, Yang LH, Kegeles LS, Susser ES, Lieberman JA (2022): Neurodegenerative model of schizophrenia: Growing evidence to support a revisit. Schizophr Res 243:154–162.